Fluids confined to narrow pores: A low-dimensional approach

Albert J. Post
Department of Chemical and Petroleum Engineering, University of Pittsburgh, Pittsburgh, Pennsylvania 15261

David A. Kofke*
Department of Chemical Engineering, State University of New York at Buffalo, Buffalo, New York 14260
(Received 3 June 1991; revised manuscript received 5 September 1991)

A fluid physisorbed in a narrow pore forms a nearly one- or two-dimensional monolayer, depending on the pore geometry, when the characteristic dimension of the pore is only slightly larger than the molecular size. In such cases, previous work shows that the average density of an adsorbed phase in equilibrium with a bulk phase can be predicted by treating the adsorbate as a low-dimensional (low-D) fluid, when the adsorbate density is low. For example, a fluid of hard spheres adsorbed inside a narrow planar pore resembles a fluid of hard disks. We improve the low-D model by regarding the adsorbate as a polydisperse fluid constrained to a lower dimension; thus, molecular size in the lower-dimensional space replaces the adsorbate position in the dimension normal to the adsorbate surface in the true geometry. The size distribution in the pseudo-low-D mixture is not chosen arbitrarily, but specified by the equilibrium condition between the low-D mixture and the bulk fluid. This equilibrium condition follows naturally from the formalism of the semigrand canonical ensemble, which provides a convenient thermodynamic description of polydisperse mixtures. The mapping of the adsorbed phase onto a polydisperse low-D fluid is examined for examples of hard-particle fluids. We report the average adsorbate density relative to the density of a bulk fluid in equilibrium with the adsorbed phase. The polydisperse low-D model provides a better representation of dense adsorbed layers than the simpler low-D model throughout the entire range of applicability of the models, as demonstrated by comparison to Monte Carlo simulations. The theory also fares better than a well-regarded smoothed density-functional theory in predicting density profiles for hard spheres in very-narrow-slit pores.

PACS number(s): 61.20.−p, 64.60.Cn, 68.45.Ax

I. INTRODUCTION

A fluid permeating a porous solid may differ markedly from a bulk fluid in structure and, consequently, in thermodynamic properties, if the molecular dimensions are comparable to the characteristic dimensions of the pores. The thermodynamics of fluids confined to narrow pores is relevant to a variety of physical phenomena including gas adsorption in porous media, capillary condensation, chromatography, membrane transport, tertiary oil recovery, and adsorption in soil. Here, we employ theory and computer simulation to examine physisorbed molecular systems that are strongly confined [1]; that is, at least one of the spatial dimensions available to the adsorbate molecules is so restricted that the adsorbed fluid resembles a one- or two-dimensional film, depending on the adsorbent geometry. Natural examples of two-dimensional adsorbed layers are found in the interstices of layered compounds like clays and hydrotalcites [2]. The structure of zeolite compounds [3] and a recently synthesized antimony sulfide compound [4] possess molecular-sized channels that could impose a nearly one-dimensional geometry on adsorbed molecular fluids. Solutions of colloidal material in narrow channels of fabricated membranes provide further examples of a one-dimensional adsorbed layer [5]. Strong sorbent-sorbate enthalpic effects can play a role in restricting the adsorbate, but the obvious examples of low-dimensional fluids are realized in nature because of geometric restrictions imposed by the adsorbent. For our purposes, a strongly confined fluid occupies a pore with a characteristic dimension D less than two times the molecular size d.

Considerable theory and computer-simulation studies have focused in recent years on the structure and thermodynamic properties of fluids confined to narrow pores [6–14]. Adams and co-workers [1] have examined strongly confined or quasi-two-dimensional films of Lennard-Jones fluids confined to slit pores. They found that an integral equation (specifically, the compressibility sum rule) requires that the local density conform to a simple universal two-parameter function for any molecular fluid adsorbed in any pore that imposes a two-dimensional (2D) order on the adsorbate. Tarazona, Marconi, and Evans [15] have constructed a density-functional theory (DFT) of fluids in a narrow slit from the free energy for a hard-disk fluid. They used this theory to check their more-general smoothed DFT for adsorbed fluids. Some years earlier, Glandt [16] developed a virial-type series for the pore bulk-distribution coefficient in powers of the bulk density, and he calculated the second and third surface virial coefficients for hard-sphere solutes in regular geometric pores. As part of the same work, Glandt proposed a treatment in which the adsorbed phase is modeled as a one- or two-dimensional fluid when confined to very narrow cylindrical or planar pores, respectively. The purpose of the present work is to refine this low-dimensional (low-D) approach to strongly confined fluids.

A partition coefficient defines the equilibrium ratio of molecular concentration in the adsorbed phase to that of a bulk phase of the same fluid, and it is determined from the condition of equilibrium between the phases—equality of temperature and chemical potential. For convenience, we work with the *activity a* instead of the chemical potential μ; these are related by

$$kT \ln a = \mu - \mu_0 \tag{1.1}$$

where T is the absolute temperature, k is Boltzmann's constant, and μ_0 is the chemical potential of the standard state: the ideal-gas bulk phase at unit molecular concentration and the same temperature. The equilibrium criterion of equality of chemical potentials can be replaced directly by equality of activities.

The bulk activity can be written

$$a_b = \rho_b \gamma_b \tag{1.2}$$

where ρ_b is the bulk density and γ_b is the bulk activity coefficient, which is a known function of ρ_b. Thus specification of the bulk density determines the activity of both phases. The adsorbed-phase activity can be formally decomposed into a part that accounts for in-plane cooperative effects and a part due to the specific interactions between one adsorbate molecule and the adsorbent [16,17]. The former part can be related to an adsorbed-phase activity coefficient γ, while the latter is simply the inverse of Henry's constant H for adsorption. With this modification, the equilibrium condition becomes

$$\frac{1}{H}\rho\gamma = \rho_b \gamma_b \tag{1.3}$$

where the adsorbed phase density ρ is defined per unit volume of pore space. We emphasize that ρ and γ in *this* relation are average properties for the entire pore, and not local properties that vary with position. Equation (1.3) can be rearranged to give the partition coefficient K,

$$K \equiv \frac{\rho}{\rho_b} = H\frac{\gamma_b}{\gamma} . \tag{1.4}$$

Glandt suggested that for pores with $D < 2d$, γ can be closely approximated by the activity coefficient of a low-dimensional fluid. In the two example cases he considered, hard spheres adsorbed in a cylindrical pore and hard spheres adsorbed in a slit pore, γ is modeled as a 1D-fluid activity coefficient and a 2D-fluid activity coefficient, respectively. Each low-dimensional activity is a function of an effective low-dimensional density n (i.e., per unit area or unit length, as appropriate). Purely geometric considerations dictate that, for the cylindrical pore geometry

$$n = \frac{\pi}{4} D^2 \rho , \tag{1.5}$$

where D is the pore diameter; and, for the slit pore geometry

$$n = D\rho , \tag{1.6}$$

where D here is the distance between the parallel pore walls. The low-dimensional theory becomes exact in the limit as D approaches d, since sorbate-sorbate interactions act parallel to the adsorbent surface. Glandt did not have computer-simulation results available to verify his theory, but MacElroy and Suh [18] have since reported a Monte Carlo (MC) simulation study for hard spheres in cylindrical pores. Their results together with our own MC simulations reveal that at modest bulk densities, Glandt's low-dimensional theory provides a good approximation for the average adsorbed-phase density up to pore widths near the limit of its applicability, $D = 2d$. However, at higher bulk densities the treatment considerably underestimates the partition coefficient near the limiting pore width, and so there is room for improvement.

A logical way to build upon the low-dimensional model is to introduce the notion of polydispersity: the strongly confined adsorbed phase becomes a pseudo mixture of low-dimensional molecules. A polydisperse fluid represents the continuous limit of a discrete mixture, in which the composition is described in terms of a distribution function rather than a set of mole fractions [19–21]. The distribution of sizes in the low-dimensional space compensates for the neglect of the molecular coordinate normal to the adsorbent surface, yet the low-dimensional mixture is easier to model than the true interfacial fluid. We will refer to Glandt's low-dimensional model as the monodisperse approach to distinguish it from our polydisperse approach.

The appropriate formalism for using a low-dimensional polydisperse mixture model to treat confined fluids is provided by the semigrand ensemble. The formalism and its role in the theory are described in Sec. II. The treatment is inexact, so several approaches may be devised; we will discuss three of them in Sec. III. In Sec. IV the methods are applied to a fluid of hard disks confined between narrowly spaced lines, the two-dimensional analog of a narrow pore. The different approaches are evaluated by comparison to computer simulation. Section V extends the theory to hard-sphere systems in slitlike and cylindrical pores, and also compares the theoretical results to simulation. Conclusions and the extensions of the theory are discussed in Sec. VI.

II. THEORY

A. Model system

For clarity, we develop and implement the semigrand mixture approach for a specific, simple model system: a bulk fluid of hard disks in equilibrium with a fluid of disks confined between two bounding lines. This is the two-dimensional analog of a fluid of spheres in equilibrium with an adsorbed phase confined to either slit-shaped or cylindrical pores. While exceedingly simple, this disks-between-lines model contains enough of the elements of the general problem to allow us to demonstrate our approach.

The bounded fluid is referred to as the narrow hard-disk system, or simply the adsorbed phase. We restrict the separation D between the lines (i.e., the pore width) to be less than or equal to $2d$, where d is the disk diameter (Fig. 1). We let x_i and y_i be the axial and radial coordi-

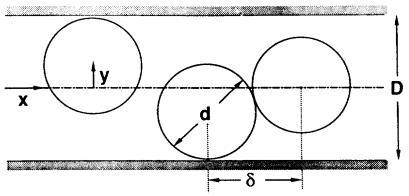

FIG. 1. Coordinate system and parameters used in description of confined fluid.

nates, respectively, of the center of disk i, with y_i defined as zero along the centerline of the pore. The lines merely confine the fluid of disks, and so the pore-wall interaction is one of simple hard repulsion. As a result, the radial coordinates are confined to the domain $-(D-d)/2 \le y \le +(D-d)/2$. Additionally, for pore widths $D \le (1+\sqrt{3}/2)d$, interactions are possible only between adjacent disks; we denote this pore width as $D_{\rm NN}$. Second-nearest-neighbor interactions are possible in the domain $D_{\rm NN} \le D \le 2d$.

The restriction $D < 2d$ prevents disks from passing one another along the pore, and so the adsorbed phase resembles a one-dimensional fluid of hard rods. The axial component of the distance of closest approach of two disks corresponds to the collision diameter of two hard rods. This collision diameter depends on the radial coordinates of the two disks, and so it is appropriate to use a polydisperse hard-rod *mixture* to model the adsorbed phase. We define $\delta(y,y')$ as the distance of closest approach, projected onto the pore axis, of two adjacent disks having radial coordinates y and y':

$$\delta(y,y')=[d^2-(y-y')^2]^{1/2} . \tag{2.1}$$

The disks freely sample radial coordinates, so we must work within a framework in which the hard-rod mixture freely samples rod lengths. The appropriate formalism is provided by the semigrand ensemble.

B. The semigrand ensemble

The semigrand canonical free energy Y is a Legendre transform of the (canonical) Helmholtz free energy A [21,22]. For a polydisperse hard-rod mixture

$$\beta Y \equiv \beta A - \int N(\sigma)\beta\Delta\mu(\sigma)d\sigma = -\beta PL + N\beta\mu(\sigma_0) \tag{2.2}$$

where L is the length of the system, P is the 1D pressure, N is the total number of rods, and $\beta = 1/kT$. The functions $N(\sigma)$ and $\mu(\sigma)$ represent the number and chemical-potential distributions, respectively, of rods of diameter (i.e., length) σ, while the difference $\Delta\mu$ is $\mu(\sigma)-\mu(\sigma_0)$, where σ_0 is the diameter of an arbitrarily chosen reference species; the integration is over all rod lengths being modeled. The last equality in Eq. (2.2) is due to Euler's formula.

The definition of the activity given in Eq. (1.1) may be extended to a component of the polydisperse mixture. Accordingly, we write $a(\sigma)$, the activity of the component with diameter σ, as

$$\ln a(\sigma) \equiv \beta\mu(\sigma) - \ln\Lambda^2 \tag{2.3}$$

where Λ is its thermal de Broglie wavelength of the two-dimensional system of disks being modeled; we have neglected here any internal molecular degrees of freedom. With this definition, the fundamental differential equation in this ensemble is

$$d(\beta Y) = Ud\beta - \beta PdL + \beta\mu(\sigma_0)dN - \int N(\sigma)\delta\ln[\alpha(\sigma)]d\sigma \tag{2.4}$$

where U is the internal energy, and $\alpha(\sigma)$ is the activity ratio $a(\sigma)/a(\sigma_0)$. The independent variables in this ensemble are the temperature, density, and the activity-ratio distribution. We emphasize that the mixture composition is a *dependent* variable in the semigrand ensemble. This *a posteriori* nature of the mixture composition is consistent with the way fluids in pores behave physically: the inhomogeneous distribution of molecules in the pore is not an independent quantity but, instead, depends on the geometry and physics of the particle-particle and particle-wall interactions.

The analogy between a semigrand mixture and a confined fluid is clarified by comparison of their corresponding partition functions. The semigrand partition function for the low-dimensional analog of the adsorbed phase is

$$\exp(-\beta Y) = \frac{1}{\Lambda^{2N}N!}\int_{(N)} d\sigma^{(N)} \int_{(N)} dx^{(N)} \exp(-\beta U) \times \prod_{i=1}^{N} \alpha(\sigma_i) . \tag{2.5}$$

The notation (N) is used to represent an integral for each of the N molecules, e.g., $\int_{(N)} d\sigma^{(N)} \equiv \int d\sigma_1 \int d\sigma_2 \cdots \int d\sigma_N$. The *canonical* partition function of the adsorbed phase is

$$\exp(-\beta A) = \frac{1}{\Lambda^{2N}N!}\int_{(N)} dy^{(N)} \int_{(N)} dx^{(N)} \exp(-\beta U) \times \prod_{i=1}^{N} \exp[-\beta V(y_i)] \tag{2.6}$$

where $V(y)$ is the external field imposed by the boundaries. In our case, the external field is just the hard-particle–wall repulsion, which restricts the radial positions to the domain $|y| \le (D-d)/2$. The hard rods sample coordinates along the identity axis (σ) just as the adsorbed hard disks sample the radial coordinates (y). The activity ratio $\alpha(\sigma)$ determines the distribution of rods in composition space just as the external field influences the position of the disks in the radial coordinate. To complete the analogy we must define $\alpha(\sigma)$ so that it has the same normalization as $\exp[-\beta V(y)]$; thus for the present system

$$\int \alpha(\sigma)d\sigma = D-d \tag{2.7}$$

where the integration is performed over all diameters needed to model the adsorbed phase.

It is convenient to describe the composition of a po-

lydisperse mixture by a distribution function $p(\sigma)=N(\sigma)/N$, which is normalized to unity. Further, we define $f(y)$ as a distribution function in position space that is equal to $\rho^{(1)}(y)/n$, where $\rho^{(1)}(y)$ is the (inhomogeneous) singlet density function inside the pore [23], and $n=N/L$ is the 1D number density; $f(y)$ is also normalized to unity. The component activity coefficient in the adsorbed phase is defined

$$\gamma(\sigma)=\frac{a(\sigma)}{np(\sigma)} . \tag{2.8}$$

The semigrand partition function, Eq. (2.5), describes a one-dimensional mixture of rods, each characterized by an individual molecular diameter, while the collision diameter of each pair of rods is given by the arithmetic mean of their molecular diameters. However, Eq. (2.1) specifies the equivalent hard-rod-collision diameter of a pair in a way that cannot be broken up into the sum of two terms, each containing only y or y'; therefore, an equivalent molecular diameter cannot be uniquely defined as a function of the radial coordinate. This fundamental incongruity precludes an isomorphism between the narrow hard-disk system and a hard-rod mixture. To proceed further, we develop approximate techniques to map the adsorbed phase onto a hard-rod mixture.

Thus the central modeling question of our theory may be stated as follows: given a set of coordinates $\{y\}$ representing the radial positions of all disks in a particular configuration of the narrow hard-disk system, how do we map this into a set of *molecular* diameters of a hard-rod system so that the equilibrium properties of the adsorbed phase are best described? We have devised two approaches, described in Secs. III A and III B, respectively. Before turning to them, we deal with the more general problems of how the activity-ratio distribution is specified and how equilibrium with the bulk phase is incorporated in the semigrand approach.

C. Specification of activity ratios

Once a mapping of disk radial coordinates to rod diameters has been defined, the appropriate choice for the semigrand hard-rod activity-ratio distribution is easily established. This distribution is determined solely by the choice of the mapping and by the geometry of the system (and by pore-wall interactions for the general case). In particular, it does not depend on the densities of the adsorbed or bulk phases. Consequently, the low-density limit of the adsorbed phase determines the appropriate form for $\alpha(\sigma)$. As the adsorbed-phase density tends to zero, the disks distribute themselves uniformly across the accessible width of the pore, the component activity coefficients of the effective hard-rod mixture tend to unity, and the activity-ratio distribution coincides with the (unnormalized) composition of the hard-rod mixture

$$\alpha(\sigma)=\lim_{\rho\to 0}\frac{p(\sigma)}{p(\sigma_0)} . \tag{2.9}$$

Therefore the appropriate activity-ratio distribution to use in modeling the adsorbed phase is proportional to the hard-rod mixture composition that corresponds to a uniform radial distribution of disks. The definition is made complete by the normalization condition, Eq. (2.7).

Once the activity-ratio distribution has been specified, evaluation of the mixture composition is straightforward. In terms of the composition and the hard-rod mixture activity coefficient, the activity ratio is

$$\alpha(\sigma)=\frac{p(\sigma)\gamma(\sigma)}{p(\sigma_0)\gamma(\sigma_0)} \tag{2.10}$$

from which we have

$$p(\sigma)=\frac{\alpha(\sigma)/\gamma(\sigma)}{\int\alpha(\sigma)/\gamma(\sigma)d\sigma} \tag{2.11}$$

where we have used normalization of $p(\sigma)$ to unity to eliminate the terms in σ_0. The particle distribution $f(y)$ in the pore is found from this composition by inverting the mapping.

D. Equilibrium with the bulk phase

The density of particles in the pore must be evaluated as a function of the density of the bulk phase using the criterion of equality of chemical potentials between the two phases. The adsorbed phase is modeled as an effective one-dimensional mixture, so we must specify which species chemical potential is equated to that of the bulk. As given by Eq. (2.4), the work of inserting a particle into a semigrand mixture, $(\partial Y/\partial N)_{T,V,\Delta\mu}$, is the chemical potential of the reference component, $\mu(\sigma_0)$, where σ_0 is simply that component for which the imposed activity ratio $\alpha(\sigma)$ is unity. This chemical potential must be equated to the work of removing a particle from the bulk, the bulk chemical potential μ_b. Equivalently,

$$a(\sigma_0)=a_b . \tag{2.12}$$

From Eq. (2.8), the reference component activity is

$$a(\sigma_0)=np(\sigma_0)\gamma(\sigma_0) . \tag{2.13}$$

Since $\alpha(\sigma_0)=1$ by definition, we may combine Eqs. (2.11)–(2.13) to write the equilibrium relation in its final form

$$\frac{n}{\int\alpha(\sigma)/\gamma(\sigma)d\sigma}=a_b . \tag{2.14}$$

We note that σ_0 has been eliminated from this expression.

III. MAPPINGS

We now turn to the task of selecting transformations that map the narrow hard-disk fluid into a polydisperse hard-rod mixture. Two approaches may be identified: (1) a mapping of the *distribution* of radial coordinates into a *distribution* of hard-rod diameters; and (2) a mapping of *individual* radial coordinates into *individual* hard-rod diameters.

A. Distribution mappings

A given distribution of radial coordinates $f(y)$ corresponds unambiguously—via Eq. (2.1)—to a unique distribution of hard-rod-collision diameters $p_c(\delta)$. Using standard methods from probability theory [24], we may in turn use $p_c(\delta)$ to extract an appropriate distribution of molecular diameters $p(\sigma)$. If we consider δ to be a random variable that is the arithmetic mean of two other random variables σ and σ', each distributed independently according to $p(\sigma)$, then the distribution $p_c(\delta)$ is given by

$$p_c(\delta)=\int p(\sigma)p(2\delta-\sigma)d\sigma \tag{3.1}$$

with integration limits given by the domain of $p_c(\delta)$. In our application $p_c(\delta)$ is known, and we must invert this convolution to extract $p(\sigma)$, which we then use for the activity-ratio distribution $\alpha(\sigma)$.

As prescribed by Eq. (2.9), the activity-ratio distribution is determined by studying the ideal-gas limit. If the disks are distributed uniformly in the accessible area of the pore, then the distribution of hard-rod-collision diameters is

$$p_c(\delta)=\begin{cases}(D-d)\delta\left[\dfrac{1}{(d^2-\delta^2)^{1/2}}-\dfrac{1}{D-d}\right], & \delta_m\le\delta\le d\\ 0 \quad \text{otherwise} .\end{cases} \tag{3.2}$$

The minimum collision diameter $\delta_m=[D(2d-D)]^{1/2}$ corresponds to adjacent disks occupying opposite sides of the pore; according to Eq. (3.1) it also represents the minimum molecular diameter. The distribution $p_c(\delta)$ given here has already been normalized such that the corresponding $p(\sigma)$ from Eq. (3.1) normalizes to $D-d$ (see Appendix A). Unfortunately, there is no function $p(\sigma)$ that satisfies Eq. (3.1) for $p_c(\delta)$ given by Eq. (3.2): we show in Appendix A that these relations require $p(\sigma)$ to obey several conditions, some of which are in contradiction. Nevertheless, we may select the most important of these conditions to construct an approximate distribution which is suitable for our analysis.

First, $p(\sigma)$ must be normalized to $(D-d)$; second, the first moment of $p(\sigma)$ must be equal to $2/(D-d)$ times the first moment of the distribution given to Eq. (3.2); third, $p(\sigma)$ must diverge with an exponent of $-\frac{3}{4}$ as $\sigma\to d$; finally, the domain of σ must be the same as that for δ, given in Eq. (3.2). A simple form may be constructed to satisfy these conditions, and from Eq. (2.9) we identify the result as the activity-ratio distribution, thus

$$\alpha(\sigma)=\begin{cases}\dfrac{a}{(d-\sigma)^{3/4}}+b, & \delta_m\le\sigma\le d\\ 0 \quad \text{otherwise}\end{cases} \tag{3.3}$$

where the constants a and b in this equation are chosen to satisfy the conditions listed above; they are functions only of the ratio D/d.

With $\alpha(\sigma)$ given by Eq. (3.3), Eqs. (2.11) and (2.14) may be combined to determine the density n and composition $p(\sigma)$ of the effective hard-rod mixture that best models the adsorbed phase in equilibrium with a bulk phase of activity a_b. With Eq. (1.6), the adsorbed-phase density ρ is easily recovered from these results

$$\rho=n/D . \tag{3.4}$$

Numerical results and comparison with simulation are presented in Sec. IV.

B. Individual mappings

The treatment is simplified considerably if the mapping provides a one-to-one correspondence between each disk's radial coordinate and its effective hard-rod diameter. We will develop a general approach to such mappings, demonstrate its use with a very simple mapping, and then go on to discuss a more sophisticated and effective choice.

If $\sigma(y)$ is a single-valued function that gives the effective hard-rod diameter as a function of the disk radial coordinate, then any distribution $f(y)$ in the radial coordinate is easily transformed into a diameter distribution $p(\sigma)$ by [24]

$$p(\sigma)=2f(y)\left|\frac{dy}{d\sigma}\right| \tag{3.5}$$

where the bars represent the absolute value, and the factor of 2 accounts for the axial symmetry of the pore.

The activity-ratio distribution of the hard-disk mixture is obtained when $f(y)$ in Eq. (3.5) is uniform; thus, when normalized according to Eq. (2.7),

$$\alpha(\sigma)=2\left|\frac{dy}{d\sigma}\right| . \tag{3.6}$$

We delay evaluating the derivative because it drops out when this equation is inserted into the equilibrium equations developed in Sec. II. In particular, Eq. (2.11) when combined with Eq. (3.6) becomes

$$p(\sigma)\left|\frac{d\sigma}{dy}\right|=\frac{1}{\gamma(\sigma)\int\gamma^{-1}(\sigma)|dy/d\sigma|d\sigma} \tag{3.7}$$

with integration limits that depend on the specific mapping. We divide Eq. (3.7) by 2. Then, according to Eq. (3.5), the left-hand side is $f(y)$, and the integral over σ can be transformed into an integral over y covering half the accessible pore width; with the factor of 2 this may be written as an integral over the full accessible pore width, yielding

$$f(y)=\frac{1}{\gamma(\sigma(y))\int_{-(D-d)/2}^{(D-d)/2}\gamma^{-1}(\sigma(y))dy} . \tag{3.8}$$

All subsequent integrals over y will be written with these integration limits implicit. Equation (2.14) may be modified in a similar fashion,

$$\frac{n}{\int\gamma^{-1}(\sigma(y))dy}=a_b . \tag{3.9}$$

A compact expression of the treatment is found by combining Eqs. (3.8) and (3.9):

$$nf(y)\gamma(\sigma(y))=a_b \ . \tag{3.10}$$

The left-hand side of this expression gives the activity of a disk as a function of its radial position; the equation is merely a statement that this activity is uniform and equal to the bulk activity.

As a very simple example of an individual mapping, let us define the effective rod diameter of a disk as the length of its intersection with the centerline of the pore, thus

$$\sigma(y)=[d^2-(2y)^2]^{1/2} \ . \tag{3.11}$$

The hard-rod activity coefficient is given exactly by [20,25]

$$\ln\gamma(\sigma)=-\ln(1-ns_1)+\frac{n\sigma}{1-ns_1} \tag{3.12}$$

where s_1 is the first moment of the distribution of diameters,

$$s_1=\int_{\delta_m}^{d}\sigma p(\sigma)d\sigma \tag{3.13a}$$

or, equivalently, the average effective 1D diameter weighted by the distribution of disks in position space,

$$s_1=\int\sigma(y)f(y)dy \tag{3.13b}$$

where δ_m in Eq. (3.13a) is the same as defined for Eq. (3.2). With this result, Eq. (3.10) becomes

$$\frac{nf(y)}{1-ns_1}\exp\left[\frac{n[d^2-(2y)^2]^{1/2}}{1-ns_1}\right]=a_b \ . \tag{3.14}$$

The solution to Eqs. (3.12)–(3.14) as a function of a_b is presented in Sec. IV.

A more sophisticated individual mapping is

$$\sigma(y)=\int f(y')\delta(y,y')dy' \tag{3.15}$$

where $\delta(y,y')$ is defined in Eq. (2.1). In this case, the effective 1D molecular diameter is a functional of the identity distribution. Equation (3.10) still determines the equilibrium identity distribution, but the activity coefficient of a component in the mixture will no longer be represented by Eq. (3.12). As described in Appendix B, the appropriate expression for the activity coefficient is

$$\ln\gamma[\sigma(y)]=-\ln(1-ns_1)+\frac{2n\sigma(y)-ns_1}{1-ns_1} \ . \tag{3.16}$$

The equilibrium condition results from combination with Eq. (3.10),

$$\frac{nf(y)}{1-ns_1}\exp\left[\frac{n(2\sigma(y)-s_1)}{1-ns_1}\right]=a_b \ . \tag{3.17}$$

Equation (3.17) is an implicit relation for the distribution of disk positions. The distribution of components in the polydisperse fluid and the overall density n can now be determined by successive substitution. The procedure is described in Sec. IV.

IV. APPLICATION: CONFINED DISKS

We apply the low-D polydisperse theory with the mappings described in the proceeding section to the fluid of hard disks confined between parallel lines. The mappings are compared to one another, a monodisperse low-D theory, and computer simulation in Figs. 2(a) and 2(b). The figures display the partition coefficient, $(n/D)/\rho_b$, obtained by the different methods as a function of relative pore width, D/d, for bulk densities of $\rho_b d^3=0.3$ and 0.6, respectively. These calculations are discussed in detail below. A bulk fluid of hard disks is in equilibrium with the adsorbed phase, so all of our calculations employ the same bulk-phase activity. We adopt the expression

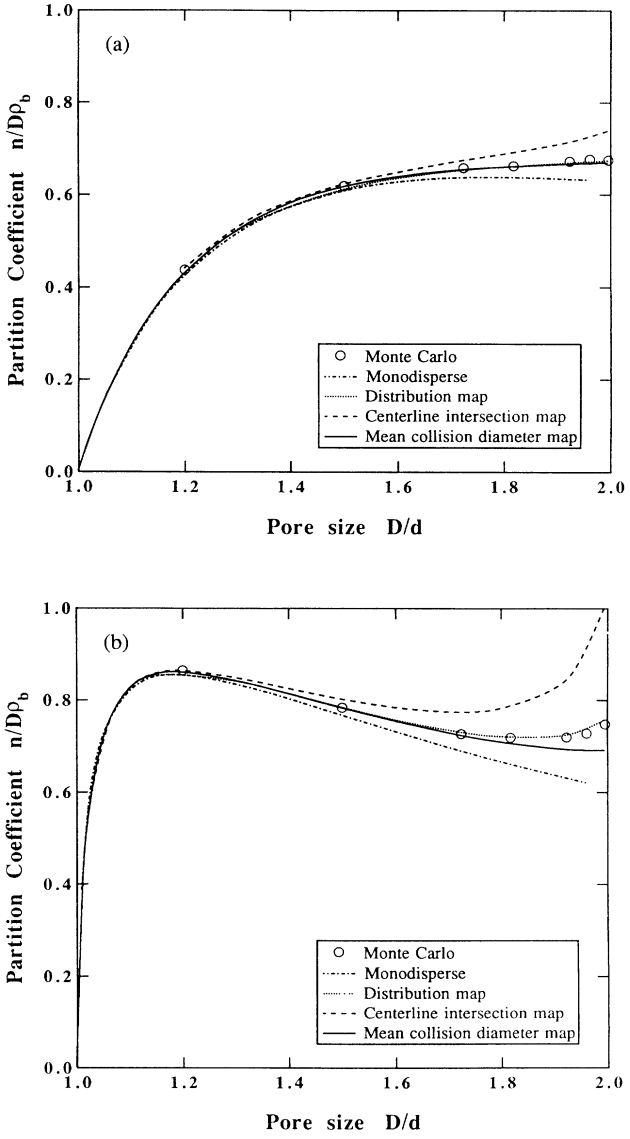

FIG. 2. Partition coefficients as a function of pore diameter for adsorbed phase of disks between lines. Grand canonical Monte Carlo results are indicated by the circles, and the various implementations of the low-dimensional theories are given by the lines. (a) Bulk density $\rho_b=0.3$; (b) $\rho_b=0.6$.

$$a_b=\frac{\rho_b}{(1-\eta)^{0.743}}\exp\left[\frac{1.257}{1-\eta}-0.043\left[1-\eta+\frac{\eta^4}{(1-\eta)^3}\right]+\frac{0.9785+0.128\eta^2}{(1-\eta)^2}-2.1925\right] \tag{4.1}$$

as the hard-disk fluid activity, where $\eta=\pi\rho_b d^2/4$ is the bulk-phase packing fraction. Equation (4.1) was derived by Glandt [16] using a hard-disk equation of state proposed by Henderson [26].

The *monodisperse* low-D theory models the adsorbed phase as a fluid of hard rods of length d. The approach employs Eq. (1.4) with $\gamma_b=a_b/\rho_b$ and a_b given by Eq. (4.1), while the adsorbed-phase activity coefficient is

$$\ln\gamma=-\ln(1-nd)+\frac{nd}{1-nd}\ , \tag{4.2}$$

which follows from the equation of state for hard rods [27]. The Henry's constant is

$$H=1-\frac{d}{D} \tag{4.3}$$

for this geometry, which is simply the fraction of the pore volume accessible to the center of the disk. Equation (1.4), with these substitutions, is easily solved for n using Newton's method when ρ_b is specified. Glandt [16] first used the monodisperse theory to calculate partition coefficients for hard spheres in slits or cylindrical pores, but he did not consider the confined hard-disk fluid.

Our *distribution* mapping for the polydisperse low-D theory uses Eq. (3.3) as the activity-ratio distribution $\alpha(\sigma)$ that approximately satisfies Eqs. (3.1) and (3.2). The constants a and b, as a function of D/d, are determined numerically to satisfy zeroth- and first-moment criteria as described in Sec. III A and Appendix A; this operation merely requires the solution of two linear equations in a and b. With this specification for $\alpha(\sigma)$, and with $\gamma(\sigma)$ given by Eq. (3.12), Eq. (2.11) provides the estimate of the effective hard-rod composition $p(\sigma)$. This is an implicit expression, because $\gamma(\sigma)$ depends on the first moment of $p(\sigma)$. A numerical solution is easily obtained by reducing Eqs. (2.11), (2.14), (3.12), and (3.13) to two equations that are solved simultaneously for the first moment s_1 and the pore density n. The secant method works well here.

The *centerline-intersection* mapping for the polydisperse low-D theory prescribes the effective rod length of each disk as the length of its intersection with the pore centerline, Eq. (3.11). Equation (3.14) expresses $f(y)$ in terms of a_b, n and s_1; Eq. (3.13) and normalization of $f(y)$ to unity then provide two equations that are solved simultaneously for n and s_1 using the secant method.

The *mean-collision-diameter* mapping for the polydisperse low-D approach requires that we find the distribution of disk positions that satisfies Eq. (3.10) when the activity coefficient is given by Eq. (3.16) and the collision diameter is given by Eq. (3.15). We assumed an initial form for $f(y)$ at 21 discrete points across the accessible pore, and solved the set of equations by successive substitution. The curves plotted in Figs. 2(a) and 2(b) represent solutions that converged to 0.05% of the $f(y)$ value at each point. The average adsorbed density n changed by less than 0.1% when we solved for 41 discrete points across the pore, so we take this to be the accuracy of the calculations.

The performance of the theoretical methods is judged against computer simulation. We implemented a standard grand-canonical-ensemble Monte Carlo (GCEMC) algorithm [28] to obtain results for the adsorption of hard disks between narrowly spaced lines. One move of the simulation comprises a random translation of a randomly chosen disk, and either an insertion of a disk at a random point or the removal of a randomly chosen disk. If the removal step was chosen, a particle was removed with a probability equal to ρ/a_b, where a_b is determined by Eq. (4.1). If an addition step is chosen, a particle is added if it does not overlap the bounding lines or another disk. Each simulation result shown in Figs. 2(a) and 2(b) was collected for runs of at least 4×10^5 moves for systems containing at least 50 disks on average. Initial configurations were randomized with runs of 10^5 moves. The statistical uncertainty of the reported partition coefficients is less than 1% in all cases, which is smaller than the symbol size used in the figures.

All theoretical methods perform well for very narrow pores—D/d less than about 1.2. As the pore diameter increases, significant deviation from the Monte Carlo results is observed in some of the theories, particularly at high density. The monodisperse model consistently underestimates the density within the pore, behavior that is easily understood: the collision diameters of the monodisperse model are fixed at their *maximum* values, and so it cannot account for the arrangements that permit smaller particle separations and thus greater packing into the pore. In contrast, the centerline-intersection method consistently overestimates the pore density. Because the centerline-intersection diameter often represents the *smallest* possible collision diameter for a given radial coordinate, this behavior too is easily understood. Only the distribution method and the mean-collision-diameter approach perform well over the entire range of pore widths. Indeed, these methods are the only two that account for the dependence of collision diameter on *both* particle positions. In the present application, they are about equally effective, although the distribution method shows slightly better agreement with the high-density, large-pore simulation results. This slight advantage over the mean-collision-diameter approach is offset by the extensive analysis required for implementation of the distribution method (cf. Appendix A); moreover, its accuracy is not sustained when applied to other pore geometries. Nevertheless, it appears to give the best results for the disks-between-lines model system, and so we will use it to briefly examine the behavior of this model under other conditions.

In Fig. 3(a) the partition coefficient predicted by the distribution method is plotted as a function of pore diameter for four bulk densities, and in Fig. 3(b) it is plotted

versus bulk density for four pore diameters. The behavior at low bulk density is rather unremarkable, but at higher densities interesting features emerge. Referring to Fig. 3(a), the partition coefficient peaks sharply just beyond a pore size of one disk diameter, decreases as the pore width is increased, and begins to rise again as the width approaches two diameters. This behavior is a reflection of how well the disks can optimally fill the pore as the pore widens. To illustrate, we include in Fig. 3(a) a curve indicating the maximum possible value of n/D; this maximum is achieved when the disks are packed perfectly within the pore, and each collision diameter has its minimum value. The curve exhibits the most significant qualitative features of the high-density plots (a quantitative comparison would require that this curve be divided by ρ_b). Clearly, this purely geometric consideration has a significant influence on the behavior of the partition coefficient at high density. Of course the sharp rise in the high-density partition coefficient as the pore width approaches $2d$ is not realistic, and results from the neglect of second-nearest-neighbor interactions. Such interactions are possible only for pore widths greater than $D_{NN}=1.866d$. As seen in Fig. 3(b), the unrealistic rise in the partition coefficient at high density is not present for pore widths less than or equal to this value.

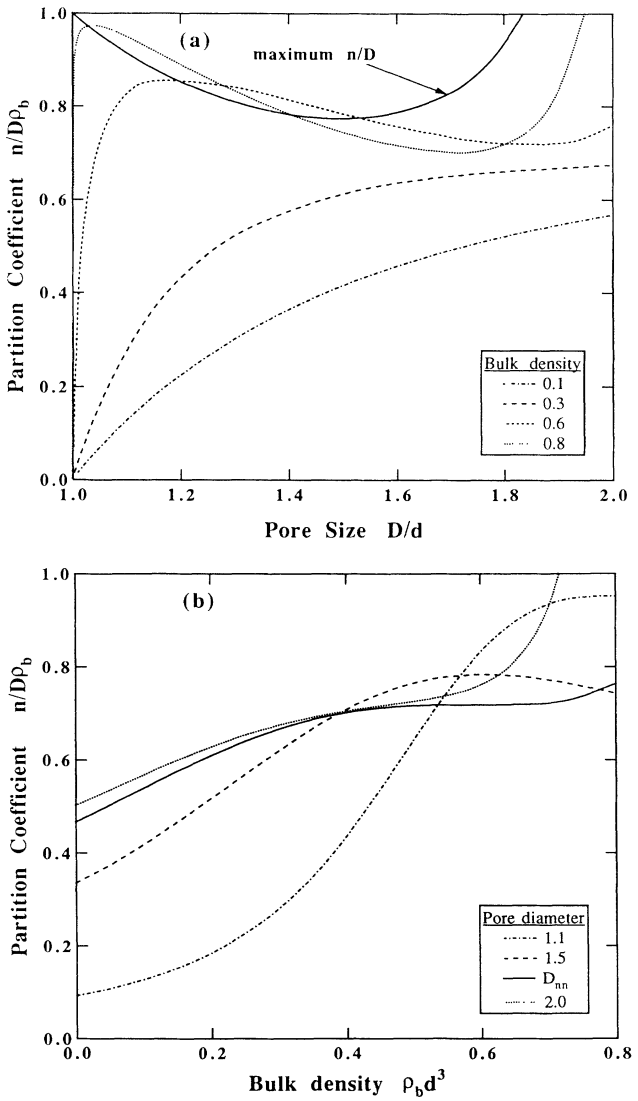

FIG. 3. Partition coefficient for the system of disks between lines, as given by the low-dimension mixture theory with the distribution mapping. Pore diameter and bulk density as indicated in (a) and (b), respectively. Solid curve in (a) indicates the maximum density n/D possible for a given pore width. This curve should be divided by the bulk density ρ_b before comparing quantitatively with the other curves.

V. OTHER GEOMETRIES

We apply the low-D polydisperse model to the partitioning of hard-sphere fluids in narrow slit-shaped pores and narrow cylindrical pores. Glandt [16] examined hard-sphere fluids in both pore geometries when he introduced the monodisperse low-D approximation. The width of the slit pore or the diameter of the cylindrical pore, both denoted by D, is less than $2d$, where d is now the diameter of hard-sphere adsorbate. Partition coefficients are determined by the mapping schemes discussed in Sec. III, and the results are compared to the monodisperse low-D approximation and GCEMC simulations. We denote those adsorbed-phase densities defined on a per volume basis (the same dimensionality as the bulk density for these examples) with the symbol ρ, and low-D densities—which are on a per area basis for slit pore and a per length basis for the cylindrical pore—with the symbol n. This format is consistent with our notation for the disks-between-lines example.

A. Hard spheres in a narrow slit

A fluid of hard spheres of diameter d confined between two walls separated by a distance $D \leq 2d$ resembles a planar two-dimensional fluid. We denote the coordinate normal to the walls as y, the radial coordinate. Application of the polydisperse low-D theory to this example requires that we map the distribution of sphere positions in the slit onto a distribution of hard-disk sizes or, alternatively, that we map the y coordinate of a sphere center onto an effective hard-disk size, $\sigma(y)$. The equations associated with the former mapping, which we referred to as a distribution mapping in Sec. III A, are applied to hard spheres in a slit and the mapping retains the same form given there. Of course, the two geometries do not have the same partition coefficients because adsorbed-phase equation of state and the bulk activities differ from those used in Sec. IV. We take the bulk activity to be that derived from the Carnahan-Starling equation of state for hard spheres [29]:

$$a_b=\rho_b \exp\left[\frac{8\eta-9\eta^2+3\eta^3}{(1-\eta)^3}\right] \tag{5.1}$$

where η is the packing fraction $\pi\rho_b d^3/6$.

Partition coefficients are also determined by the mean-collision-diameter mapping, defined by Eq. (3.15). Equa-

tion (3.10) is the equilibrium condition, with Eq. (5.1) defining a_b, but a component activity coefficient for a polydisperse mixture of hard disks is required. We construct a component activity in Appendix B for a polydisperse 2D fluid in which the effective disk size is a functional of the density distribution. The result is

$$\ln\gamma_{2D}(y) = -\ln(1-\xi_2) + \frac{2\xi_1}{\xi_0(1-\xi_2)}\frac{\delta\xi_1}{\delta N(y)} + Z\frac{\delta\xi_2}{\delta N(y)} \tag{5.2}$$

where $N(y)$ is the number density of disks occupying radial coordinate y, and Z is the 2D compressibility factor

$$Z = \frac{\beta p}{n} = \frac{1}{1-\xi_2} + \frac{\xi_1^2}{\xi_0(1-\xi_2)^2} \tag{5.3}$$

and $\xi_k = \pi n s_k/4$, with s_k the kth moment of the size distribution [cf. Eq. (3.13b)]:

$$s_k = \int dy\, f(y)[\sigma(y)]^k \tag{5.4}$$

where the integration limits are given by the accessible pore width, $-(D-d)/2$ to $(D-d)/2$. The functional derivatives of the moments are given in Appendix B.

Figure 4 compares the partition coefficients at reduced densities of $\rho_b d^3 = 0.3$ and 0.6, which are obtained from the distribution mapping and the mean-collision-diameter mapping of the polydisperse theory, the monodisperse low-D approximation, and the GCEMC simulation. The simulation results are our own since we are unaware of any previously reported MC simulations for hard-sphere fluids in slit pores of the size range of interest. Each reported simulation result was collected from MC runs of 2×10^5 moves or more for systems with an average of at least 100 adsorbed spheres. Initial configurations were randomized by runs of at least 10^5 moves. The statistical uncertainty of our GCEMC results is no more than 1% of the plotted value, which is smaller than the symbols in Fig. 4

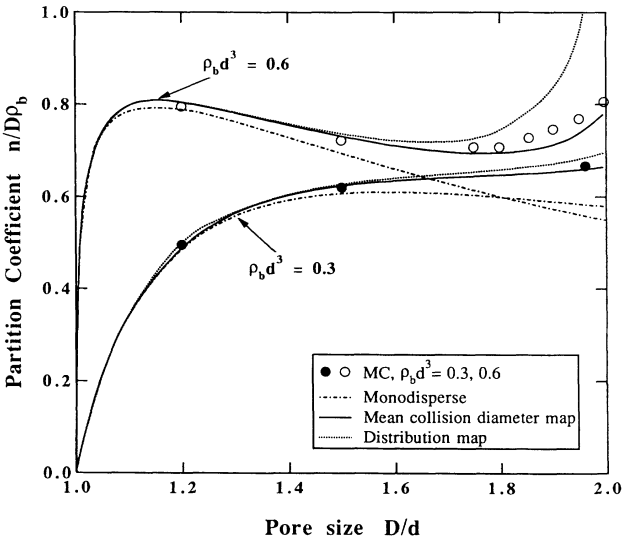

FIG. 4. Partition coefficient as a function of pore diameter for adsorbed phase of spheres in a planar slit. Grand canonical Monte Carlo results are indicated by the circles, and the various implementations of the low-dimensional theories are given by the lines.

Both polydisperse low-D approaches match the simulations for all $D \le 2d$ with $\rho_b d^3 \le 0.3$, as shown in Fig. 4. The polydisperse theory relying on the individual mapping compares favorably to the simulation results for all D of interest at $\rho_b d^3 = 0.6$, which is a considerable improvement upon the monodisperse low-D model. The polydisperse theory relying on the distribution mapping grossly overestimates the partition coefficient for $D \ge 1.8d$ at $\rho_b d^3 = 0.6$. This behavior was observed in the application described in Sec. IV, and likely arises from the neglect of second-nearest-neighbor interactions.

B. Hard spheres in a narrow cylindrical pore

A fluid of hard spheres of diameter d confined to a narrow cylindrical pore, like the confined fluid of hard disks, resembles a polydisperse one-dimensional mixture of hard rods when the pore diameter $D \le 2d$. All of the methods presented in Sec. IV can in principle be applied to this geometry. However, the ideal-gas distribution of collision diameters analogous to Eq. (3.2) cannot be obtained in closed form, and so the distribution method of Sec. III A can be applied only with great difficulty. Consequently, we do not include this method in our comparison. An equilibrium condition relating the distribution of adsorbed spheres at radial position y to the bulk fluid is given by Eq. (3.10). Equation (3.16) gives the appropriate component activity coefficient. The mean 1D collision diameter for a sphere at radial position y in the cylinder is [cf. Eq. (3.15)]

$$\sigma(y) = \int d\mathbf{y}' f(y')\delta(\mathbf{y},\mathbf{y}') \tag{5.5}$$

where $\mathbf{y}$ and $\mathbf{y}'$ define vector positions in the cylinder, and δ is the effective 1D collision diameter for spheres at positions $\mathbf{y}$ and $\mathbf{y}'$,

$$\delta(\mathbf{y},\mathbf{y}') = (d^2 - |\mathbf{y}-\mathbf{y}'|^2)^{1/2} . \tag{5.6}$$

The angular part of the integration in Eq. (5.5) is completed to yield

$$\sigma(y) = 4\pi \int dy' f(y') E(\zeta)[d^2-(y-y')^2]^{1/2} \tag{5.7}$$

with

$$\zeta = \left[\frac{4y'y}{d^2-(y-y')^2}\right]^{1/2}$$

where E is the complete elliptic integral of the second kind [30].

Partition coefficients given by the mean-collision-diameter mapping, the monodisperse low-D approximation, and computer simulations are shown in Fig. 5. MacElroy and Suh [18] have reported on some GCEMC simulations for this system, and one of their points is plotted in the figure. Our own GCEMC calculations

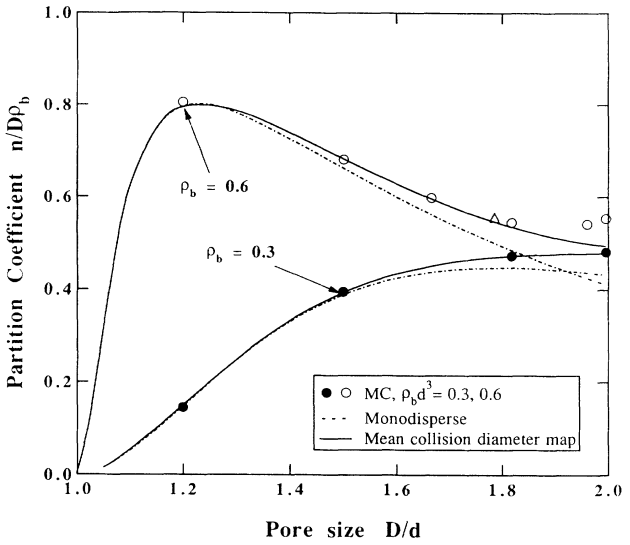

FIG. 5. Partition coefficient as a function of pore diameter for adsorbed phase of spheres in a cylindrical pore. Grand canonical Monte Carlo results are indicated by the circles, and the various implementations of the low-dimensional theories are given by the lines. The triangle is a Monte Carlo simulation result from MacElroy and Suh [18].

were verified by checking that MacElroy and Suh's partition coefficients were recovered, within the statistical uncertainty. The earlier comments pertaining to typical run lengths and statistical uncertainty of the results for slit-pore simulations apply to the cylindrical-pore simulations as well. The latter simulations contained at least 50 spheres in each case.

The polydisperse low-D theory and the simulations are nearly identical for $\rho_b d^3 \leq 0.3$ in the entire pore size range of interest, while the monodisperse low-D theory noticeably deviates from the simulation results at $\rho_b d^3 = 0.3$ for wide pores. The disparity between the theoretical approaches and the simulations occurs for smaller D with increasing density, but the polydisperse theory matches the simulations below size ratios of $D \approx 1.85d$ (approximately D_{NN}) for $\rho_b d^3 = 0.6$. GCEMC results at higher densities are difficult to obtain because insertion rates become very infrequent. This form of the polydisperse low-D theory does not capture the increase in K above $D \approx D_{NN}$. The same shortcoming was observed for the system of disks confined between parallel lines.

VI. SUMMARY AND CONCLUSIONS

We have developed a polydisperse low-D theory for strongly confined fluids, and have applied the theory to three model systems of hard-particle fluids sterically confined to narrow pores. The theory maps the adsorbed phase onto a low-D polydisperse fluid, but the mapping process is approximate, so variations may be constructed; we have considered three alternative mappings.

Adsorbed particles pack more efficiently in a narrow pore when nearest neighbors occupy positions close to opposing surfaces. We would expect high densities to impose an alternating arrangement, and this ordering is clearly easier to impose for the quasi-1D phase than for the 2D phase. In the latter case, all of the first shell neighbors about a central sphere cannot be positioned near one surface when the central sphere is near the opposing surface, since the spheres in the shell are also neighbors of each other. Thus the local distribution $f(y)$ about a given particle is not unlike the overall distribution, and we can expect in this instance the mean-collision-diameter mapping to give a good representation of the adsorbed-phase properties. The alternating arrangement possible in the quasi-1D systems reflects better packing than would be predicted by an average collision diameter approach—the local $f(y)$ differs from the overall distribution; as a consequence this theory underestimates the partition coefficient. The distribution mapping, on the other hand, is able to capture the effect of the more efficient packing, but it suffers seriously at large pore widths because of its neglect of non-nearest-neighbor interactions, which greatly attenuate the packing. The combination of ease of implementation and consistently satisfactory performance leads us to recommend the mean-collision-diameter mapping as the technique of choice from among the methods proposed here.

The theory can be extended in many ways to more complicated systems. For example, if the wall-particle interaction $V(\mathbf{y})$ is more complicated, then the activity of each component in the adsorbed phase becomes the product of the left-hand side of Eq. (3.10) and the Boltzmann factor $\exp[-\beta V(\mathbf{y})]$; for the distribution mapping, $V(\mathbf{y})$ enters through the calculation of the ideal-gas collision diameter distribution [Eq. (3.2)]. The functional form of the low-D activity coefficient remains the same. This extension of the theory permits application to adsorption on single surfaces, where $V(\mathbf{y})$ is a deep and narrow potential well. Inclusion of long-range interactions between adsorbate molecules is also possible, although the model for the low-D polydisperse phase must incorporate these interactions. Adsorption of *mixtures* may also be handled easily within the framework. To do this, we treat the species identity as another dimension, which can be included in the vector $\mathbf{y}$ [21,22]. We impose a chemical-potential-difference field in this dimension to control the composition. Anisotropic molecules may also be considered. This extension is straightforward for cylindrical, quasi-1D pores; for slit adsorption it may be necessary to have an equation of state for nonspherical disks.

To place the proposed treatment in perspective, it is of interest to compare it with established methods for treating inhomogeneous fluids. Density-functional theory [31] (DFT) has been shown in many instances to be effective in characterizing such systems. Several formulations of DFT have been developed for the treatment of wetting and adsorption at interfaces [15,32]. The method of Tarazona, Marconi, and Evans [15] is considered to be among the best of these [11]; further, it is known to produce local density profiles of hard spheres near walls in nearly exact agreement with simulation [33]. In Fig. 6 we present pore profiles for a system of spheres inside planar slits of diameter $D/d = 1.5$ and $1+\sqrt{3}/2$, respectively.

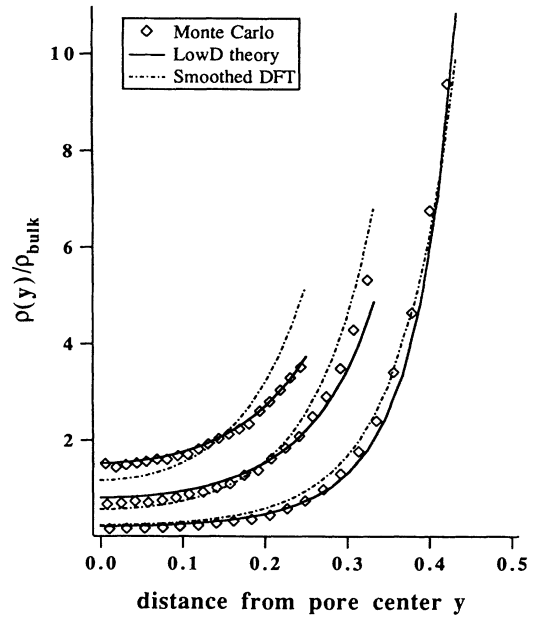

FIG. 6. Density profiles of hard spheres in slip-shaped pores, in equilibrium with a bulk fluid of density $\rho_b d^3=0.8$. The diamonds are data taken from our grand canonical Monte Carlo simulations, the solid lines represent the estimates of the proposed polydisperse low-D theory, and the broken lines are computed using the smoothed density-functional theory of Tarazona. The pore widths are, from left to right, $D/d=1.5$, 1.667, and $1+\sqrt{3}/2$, respectively.

The latter value (defined above as D_{NN}) is the pore size above which non-nearest interactions can occur, and thus represents the maximum size for which the low-D theory applies. The individual mapping described in Secs. III B and V A is used to compute the profile, and it is compared with the DFT of Tarazona and with the essentially exact profile that we determined by grand canonical Monte Carlo simulation. Both theories perform well overall, but the proposed method becomes increasingly accurate and the DFT becomes less reliable as the pore narrows. Thus we demonstrate that in the treatment of highly confined systems the proposed technique is as good as or better than the popular methods for treating inhomogenous systems. Of course, DFT methods have a much broader range of applicability, and may be applied to essentially any pore width (as well as bulk fluids). However, for the treatment of highly confined fluids, the proposed technique has greater generality; as described above, the same low-dimensional reference system may be used in a variety of situations. For this reason it may prove the technique of choice in the range of application for which it is designed.

ACKNOWLEDGMENTS

A.J.P. acknowledges support of the National Science Foundation (Grant No. CBT-8809308). D.A.K. is supported by the U.S. National Science Foundation under the Presidential Young Investigator Program (Grant No. CTS-9057161).

APPENDIX A: ANALYSIS OF DECONVOLUTION

In the distribution-mapping approach discussed in Sec. III A, the distribution of collision diameters $p_c(\delta)$ was given in Eq. (3.1) as a convolution of the distribution of molecular diameters $p(\sigma)$. In this appendix we demonstrate that for $p_c(\delta)$ given by Eq. (3.2) there exists no solution $p(\sigma)$ satisfying Eq. (3.1). We present criteria that must be obeyed by such a solution, and show that they are contradictory. Nevertheless, these criteria are useful in constructing a $p(\sigma)$ that approximately obeys Eqs. (3.1) and (3.2).

The distribution of collision diameters $p_c(\delta)$ is nonzero only for $\delta_m \le \delta \le d$; clearly $p(\sigma)$ must also be nonzero only over this domain, because a given δ represents the arithmetic mean of two values of σ and so must be bounded by these two values. Thus the limits of integration in Eq. (3.1) may be specified as a function of δ as in Fig. 7. Outside of these limits $p(\sigma)$ or $p(2\delta-\sigma)$ must be zero. Accordingly, Eq. (3.1) may be written

$$p_c(\delta)=\begin{cases}\int_{\delta_m}^{2\delta-\delta_m} p(\sigma)p(2\delta-\sigma)d\sigma\ , & \delta\le\delta_t\\ \int_{2\delta-d}^{d} p(\sigma)p(2\delta-\sigma)d\sigma\ , & \delta\ge\delta_t\end{cases} \tag{A1}$$

where $\delta_t=\frac{1}{2}(d+\delta_m)$. It is convenient to take advantage of the symmetry of the integrand and write these integrals as follows:

$$p_c(\delta)=\begin{cases}2\int_{\delta_m}^{\delta} p(\sigma)p(2\delta-\sigma)d\sigma\ , & \delta\le\delta_t\\ 2\int_{\delta}^{d} p(\sigma)p(2\delta-\sigma)d\sigma\ , & \delta\ge\delta_t\ .\end{cases} \tag{A2}$$

1. Limiting behavior of $p(\sigma)$

The value of $p(\sigma)$ at its lower limit $\sigma=\delta_m$ is easily determined by evaluating the derivative of Eq. (A2) (with respect to δ) at $\delta=\delta_m$. The result gives an expression for $p(\delta_m)$ directly,

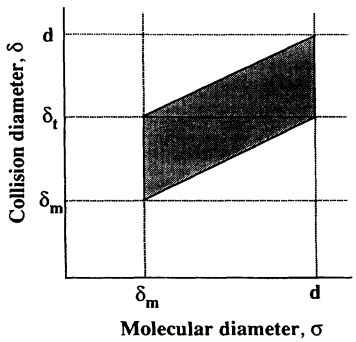

FIG. 7. Region of nonzero integrand for convolution Eq. (3.1). For a given collision diameter δ (the ordinate), the limits of integration of Eq. (3.1) are indicated by the left and right boundaries of the shaded region.

$$p(\delta_m)=\frac{1}{\sqrt{2}}\left[\left.\frac{dp_c}{d\delta}\right|_{\delta=\delta_m}\right]^{1/2} . \tag{A3}$$

With p_c given by Eq. (3.2), $p(\delta_m)$ is zero only for $D=2d$ [although $p_c(\delta_m)$ is always zero].

The behavior of $p(\sigma)$ as $\sigma\to d$ may be determined by a perturbation analysis. We define the (small) parameter $\epsilon=d-\delta$, and introduce it into Eq. (A2):

$$p_c(d-\epsilon)=2\int_0^{\epsilon} p[d-(\epsilon-s)]p[d-(\epsilon+s)]ds \tag{A4}$$

where we have defined the new dummy variable $s=\sigma-(d-\epsilon)$, and have chosen the form of Eq. (A2) that applies to $\delta\geq(d+\delta_m)/2$. We now expand $p(\sigma)$ in a series about $\sigma=d$:

$$p(\sigma)=\sum_{i=0}^{\infty} a_i(\sigma-d)^{n_i} \tag{A5}$$

where the coefficients a_i and the exponents n_i are to be determined by matching with a similar expansion of p_c. Upon substitution of this expansion, Eq. (A4) may be written in the form

$$p_c(d-\epsilon)=\sum_{i,j=0}^{\infty} a_i a_j \mathrm{B}(n_i+1,n_j+1)(2\epsilon)^{n_i+n_j+1} \tag{A6}$$

where $\mathrm{B}(n,m)=\Gamma(n)\Gamma(m)/\Gamma(n+m)$ is the beta function, with Γ the gamma function.

When p_c is given by Eq. (3.2), the expansion of $p_c(d-\epsilon)$ about $\epsilon=0$ is

$$p_c(d-\epsilon)=\frac{1}{\sqrt{2}}(D-d)\epsilon^{-1/2}-1 -\frac{3}{4\sqrt{2}}(D-d)\epsilon^{1/2}+\epsilon+O(\epsilon^{3/2}) . \tag{A7}$$

Matching exponents and coefficients of Eqs. (A6) and (A7) gives the expansion for $p(\sigma)$ about $\sigma=d$:

$$p(\sigma)=\frac{(D-d)\pi^{1/4}}{\Gamma(1/4)}(d-\sigma)^{-3/4} -\frac{1}{2\pi^{1/4}\Gamma(3/4)}(d-\sigma)^{-1/4}+O((d-\sigma)^{1/4}) . \tag{A8}$$

Thus $p(\sigma)$ has an integrable singularity at $\sigma=d$.

2. Derivative of p_c at $\delta=\delta_t$

The two right-hand sides of Eq. (A2) are equal to each other at the transition value $\delta_t=(d+\delta_m)/2$; this must be so because p_c, the function they define, is continuous here. Further, all derivatives of p_c are continuous at this point. Thus it is appropriate to examine conditions under which the derivatives of the right-hand sides of Eqs. (A2) are also continuous. If we let $p_L'(\delta)$ represent the derivative of p_c from below, while $p_H'(\delta)$ represents the derivative from above, then from Eq. (A2) we have

$$p_L'(\delta)=2[p(\delta)]^2+4\int_{\delta_m}^{\delta} p(\sigma)p'(2\delta-\sigma)d\sigma , \quad \delta\leq\delta_t \tag{A8a}$$

$$p_H'(\delta)=-2[p(\delta)]^2+4\int_{\delta}^{d} p(\sigma)p'(2\delta-\sigma)d\sigma , \quad \delta\geq\delta_t . \tag{A8b}$$

With an appropriate change of variables and an integration by parts, Eqs. (A8) can be used to relate the derivatives from above and below at $\delta=\delta_t$,

$$p_H'(\delta_t)-p_L'(\delta_t)=4p(\delta_m)p(d) . \tag{A9}$$

Thus the convolution describes a function with continuous first derivatives only if the function $p(\sigma)$ is zero at $\sigma=\delta_m$ or at $\sigma=d$. However, Eqs. (A3) and (A8) indicate that $p(\sigma)$ is *not* zero at either of these points, and in fact it diverges at one of them, hence p_L' or p_H' is infinite at δ_t. This behavior clearly is not in accord with Eq. (3.2), and so we conclude that there is no function $p(\sigma)$ that satisfies Eqs. (3.1) and (3.2).

3. Approximate form for $p(\sigma)$

Although in this instance we cannot find a $p(\sigma)$ satisfying Eqs. (3.1) and (3.2) exactly, it is possible to construct a function that obeys these equations approximately. The task is to select the most important of the exact criteria developed here, and to construct a simple function that obeys them. It has been established that the thermodynamics of hard-particle mixtures are well characterized using just the first few moments of their composition, and that the exact form of the distribution is relatively unimportant. Accordingly, we expect criteria involving the moments of $p(\sigma)$ to be relevant to any specification of an approximate function.

Equation (3.2) can be used to specify exactly the moments of any approximate $p(\sigma)$. If we define c_n and s_n as the nth moments, about the origin, of the distributions $p_c(\delta)$ and $p(\sigma)$, respectively, then

$$c_n=\frac{1}{2^{n+1}}\sum_{k=0}^{n}\binom{n}{k}s_k s_{n-k} . \tag{A10}$$

Thus for $n=0,1,2$ we have

$$c_0=\tfrac{1}{2}s_0^2 , \tag{A11a}$$

$$s_1=s_0c_1/c_0 , \tag{A11b}$$

$$s_2=s_0\left[2\frac{c_2}{c_0}-\left[\frac{c_1}{c_0}\right]^2\right] . \tag{A11c}$$

Because $p(\sigma)$ is to be used to define the activity-ratio distribution $\alpha(\sigma)$, the normalization given by Eq. (2.7) requires $s_0=D-d$, and so Eq. (A11a) specifies the normalization of $p_c(\delta)$; this was used to develop Eq. (3.2). Equations (A11b) and (A11c) then specify the moments of $p(\sigma)$. In the application to the disks-between-lines model, the adsorbed phase is characterized fully by just the first moment of the composition distribution, so we employ only Eq. (A11b) in constructing an approximate $p(\sigma)$.

To summarize, we constructed a function $p(\sigma)$ that approximately satisfies Eqs. (3.1) and (3.2) using the following criteria: (1) from Eq. (A8), $p(\sigma)$ diverges with an ex-

ponent of $-\frac{3}{4}$ as $\sigma \to d$: (2) the first moment of $p(\sigma)$ is given by Eq. (A11b), with c_0 and c_1 the zeroth and first moments of the distribution $p_c(\delta)$ given by Eq. (3.2); (3) from Eq. (2.7), $p(\sigma)$ is normalized to $D-d$. The simplest form satisfying these three criteria is that given by Eq. (3.3).

APPENDIX B: ACTIVITY COEFFICIENT FOR POLYDISPERSE ONE- AND TWO-DIMENSIONAL FLUIDS

Our mean-collision-diameter mapping [Eq. (3.15)] treats the effective size of a species as a functional of the entire component identity distribution, in contrast to the other mapping procedures which employ the standard description of hard-particle polydisperse mixtures. This unusual treatment requires that expressions for component properties such as the activity coefficient be rederived, because the functional dependence of the molecular diameters on composition leads to extra dependences on the component mole numbers. Overall mixture properties such as the pressure remain unchanged. We derive here equations for the activity coefficient of the 1D and 2D effective polydisperse fluid.

The individual mappings of Sec. III B in essence treat the adsorbed phase as a polydisperse mixture in which the radial coordinate y is the identity variable. Because the mapping of Eq. (3.15) is written in terms of $f(y)$, the distribution of radial coordinates, it is convenient to adopt this view explicitly in developing the expression for the activity coefficient $\gamma[\sigma(y)]$ needed in Eq. (3.10). Thus we shall henceforth denote this quantity simply as $\gamma(y)$, and we shall treat the adsorbed phase as a polydisperse mixture distributed in y, with a normalized composition distribution $f(y)$.

The activity coefficient $\gamma(y)$ of a component of identity y in a polydisperse mixture is given by the functional derivative [20]

$$\ln\gamma(y)=\left[\frac{\delta\beta A_r}{\delta N(y)}\right]_{T,V} \tag{B1}$$

where A_r is the residual Helmholtz free energy (i.e., that above the ideal gas at the same density) and $N(y)$ is $Nf(y)$ and is normalized to N. For the systems studied in this work, the composition dependence of A_r is expressed solely in terms of the moments of the composition ξ_n, defined

$$\xi_n=\frac{v_p}{V}\int[\sigma(y)]^n N(y)dy=v_p n s_n \tag{B2}$$

where v_p is the (generalized) volume of a particle of unit diameter (equal to unity, $\pi/4$, and $\pi/6$ in one, two, and three dimensions, respectively), and V is the system volume (or area, or length, as appropriate); s_n are the moments as defined by Eq. (5.4). Then, the activity coefficient may be given by

$$\ln\gamma(y)=\beta A_r/N+N\sum_n \frac{\partial(\beta A_r/N)}{\partial\xi_n}\frac{\delta\xi_n}{\delta N(y)} \tag{B3}$$

where the sum extends from $n=0$ to the dimensionality of the system. Normally, $\sigma(y)$ is independent of $N(y)$, and the functional derivative needed here can be written

$$\frac{\delta\xi_n}{\delta N(y)}=\frac{1}{N}\xi_0[\sigma(y)]^n . \tag{B4}$$

However, if we employ the mapping given by Eq. (3.15), then σ is itself a functional of $N(y)$. Equation (B2) is then

$$\xi_n=\frac{v_p}{VN^n}\int dy\, N(y)\left[\int N(y')\delta(y,y')dy'\right]^n \tag{B5}$$

and the functional derivative becomes

$$\frac{\delta\xi_n}{\delta N(y)}=\frac{1}{N}\xi_0\left[[\sigma(y)]^n+n\int f(y')\delta(y,y')[\sigma(y')]^{n-1}dy' - n\xi_n/\xi_0\right] . \tag{B6}$$

In particular

$$\frac{\delta\xi_0}{\delta N(y)}=\frac{1}{N}\xi_0 , \tag{B7a}$$

$$\frac{\delta\xi_1}{\delta N(y)}=\frac{1}{N}(2\xi_0\sigma(y)-\xi_1) , \tag{B7b}$$

$$\frac{\delta\xi_2}{\delta N(y)}=\frac{1}{N}\left[\xi_0[\sigma(y)]^2+2\xi_0\int f(y')\delta(y,y')\sigma(y')dy' -2\xi_2\right] . \tag{B7c}$$

For a hard-rod mixture, the residual Helmholtz free energy is [20]

$$\beta A_r/N=-\ln(1-\xi_1) . \tag{B8}$$

This relation may be inserted into Eq. (B3) and combined with Eq. (B7) to produce the expression given in Eq. (3.16). For hard disks, the result from scaled particle theory [34] leads to

$$\beta A_r/N=-\ln(1-\xi_2)+\frac{\xi_1^2}{\xi_0(1-\xi_2)} . \tag{B9}$$

Combination of Eqs. (B3) and (B9) yields Eq. (5.2).

*Author to whom correspondence should be addressed.

[1] P. A. Adams, J. R. Henderson, and J. P. R. B. Walton, J. Chem. Phys. **91**, 7173 (1989).
[2] R. E. Grim, *Clay Mineralogy* (McGraw-Hill, New York, 1968).
[3] R. M. Barrer, *Zeolites and Clay Minerals as Sorbents and Molecular Sieves* (Academic, London, 1978).
[4] J. B. Parise, Science **251**, 293 (1991).
[5] J. A. Quinn, J. L. Anderson, W. S. Ho, and W. J. Petzny, Biophys. J. **12**, 990 (1972).

[6] R. Evans, U. M. B. Marconi, and P. Tarazona, J. Chem. Phys. **84**, 2367 (1986).
[7] R. Evans, U. M. B. Marconi, and P. Tarazona, J. Chem. Soc., Faraday Trans. 2 **82**, 2376 (1986).
[8] B. K. Peterson, J. P. R. B. Walton, and K. E. Gubbins, J. Chem. Soc., Faraday Trans. 2 **82**, 1789 (1986).
[9] M. Schoen, D. J. Diestler, and J. H. Cushman, J. Chem. Phys. **87**, 5464 (1987).
[10] Z. Tan, F. Van Swol, and K. E. Gubbins, Mol. Phys. **62**, 1213 (1987).
[11] B. K. Peterson, K. E. Gubbins, G. S. Heffelfinger, U. M. B. Marconi, and F. van Swol, J. Chem. Phys. **88**, 6487 (1988).
[12] G. S. Heffelfinger, Z. Tan, U. M. B. Marconi, F. Van Swol, and K. E. Gubbins, Mol. Sim. **2**, 393 (1989).
[13] Y. Zhou and G. Stell, Mol. Phys. **66**, 767 (1989); **66**, 791 (1989).
[14] Z. Tan and K. E. Gubbins, J. Phys. Chem. **94**, 6061 (1990).
[15] P. Tarazona, U. M. B. Marconi, and R. Evans, Mol. Phys. **60**, 573 (1987).
[16] E. D. Glandt, AIChE J. **27**, 51 (1981).
[17] W. A. Steele, *The Interaction of Gases with Solid Surfaces* (Pergamon, Oxford, 1974).
[18] J. M. D. MacElroy and J.-S. Suh, AIChE Symp. Ser. **82**, 133 (1985).
[19] J. A. Gualtieri, J. M. Kincaid, and G. Morrison, J. Chem. Phys. **77**, 521 (1982).
[20] J. J. Salacuse and G. Stell, J. Chem. Phys. **77**, 3714 (1982).
[21] J. G. Briano and E. D. Glandt, J. Chem. Phys. **80**, 3336 (1984).
[22] D. A. Kofke, Ph.D. thesis, University of Pennsylvania, 1988.
[23] J. P. Hansen and I. R. McDonald, *Theory of Simple Liquids*, 2nd ed. (Academic, New York, 1986).
[24] A. Papoulis, *Probability, Random Variables, and Stochastic Processes*, 2nd ed. (McGraw-Hill, New York, 1984).
[25] J. J. Salacuse, J. Chem. Phys. **81**, 2468 (1984).
[26] D. Henderson, Mol. Phys. **34**, 301 (1977).
[27] L. Tonks, Phys. Rev. **50**, 955 (1936).
[28] D. J. Adams, Mol. Phys. **28**, 1241 (1974).
[29] N. F. Carnahan and K. E. Starling, J. Chem. Phys. **51**, 635 (1969).
[30] *Table of Integrals, Series, and Products*, edited by I. S. Gradshteyn and I. M. Ryzhik (Academic, New York, 1980).
[31] For a review of the fundamentals of density-functional theory as applied to classical fluids, see A. D. J. Haymet, Prog. Solid State Chem. **17**, 1 (1986), and references therein.
[32] E. Kierlik and M. L. Rosinberg, Phys. Rev. A **42**, 3382 (1990); Y. Rosenfeld, Phys. Rev. Lett. **63**, 980 (1989); T. F. Meister and D. M. Kroll, Phys. Rev. A **31**, 4055 (1985); W. A. Curtin and N. W. Ashcroft, *ibid.* **32**, 2909 (1985).
[33] P. Tarazona, Phys. Rev. A **31**, 2672 (1985).
[34] J. L. Lebowitz, E. Helfand, and E. Praestgaard, J. Chem. Phys. **43**, 774 (1965).

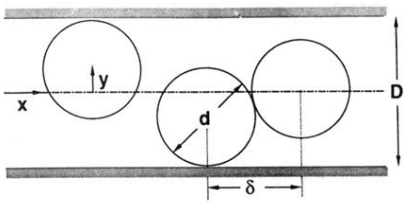

FIG. 1. Coordinate system and parameters used in description of confined fluid.

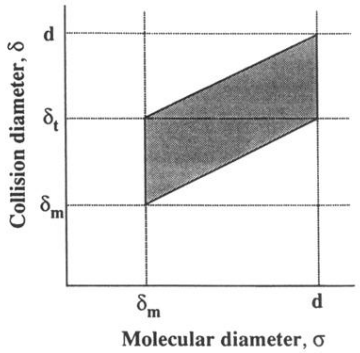

FIG. 7. Region of nonzero integrand for convolution Eq. (3.1). For a given collision diameter δ (the ordinate), the limits of integration of Eq. (3.1) are indicated by the left and right boundaries of the shaded region.